Approximate action-angle variables for the figure-eight and periodic three-body orbits

Milovan Šuvakov[*]
Institute of Physics, Belgrade University, Pregrevica 118, Zemun, P. O. Box 57, SRB-11080 Beograd, Serbia

V. Dmitrašinović[†]
Yukawa Institute for Theoretical Physics, Kyoto University, Kyoto 606-8502, Japan,
Permanent address: Institute of Physics, Belgrade University, Pregrevica 118, Zemun, P. O. Box 57, SRB-11080 Beograd, Serbia

(Received 22 June 2010; published 10 May 2011)

We use the maximally permutation-symmetric set of three-body coordinates that consist of the "hyper-radius" $R = \sqrt{\rho^2 + \lambda^2}$, the "rescaled area of the triangle" $\frac{\sqrt{3}}{2R^2}|\boldsymbol{\rho} \times \boldsymbol{\lambda}|$), and the (braiding) hyperangle $\phi = \arctan(\frac{2\rho\cdot\lambda}{\lambda^2-\rho^2})$ to analyze the "figure-eight" choreographic three-body motion discovered by Moore [Phys. Rev. Lett. **70**, 3675 (1993)] in the Newtonian three-body problem. Here $\boldsymbol{\rho}$,$\boldsymbol{\lambda}$ are the two Jacobi relative coordinate vectors. We show that the periodicity of this motion is closely related to the braiding hyperangle ϕ. We construct an approximate integral of motion $\overline{G}$ that together with the hyperangle ϕ forms the action-angle pair of variables for this problem and show that it is the underlying cause of figure-eight motion's stability. We construct figure-eight orbits in two other attractive permutation-symmetric three-body potentials. We compare the figure-eight orbits in these three potentials and discuss their generic features, as well as their differences. We apply these variables to two new periodic, but nonchoreographic, orbits: One has a continuously rising ϕ in time t, just like the figure-eight motion, but with a different, more complex, periodicity, whereas the other one has an oscillating $\phi(t)$ temporal behavior.

DOI: 10.1103/PhysRevE.83.056603 PACS number(s): 45.20.D−, 45.50.Jf

I. INTRODUCTION

The three-body problem is one of the oldest and most challenging in classical mechanics [1]. Until recently, only a few periodic three-body solutions were known [1] in Newton's gravitational interaction potential. A new periodic, "figure eight," trajectory was found in 1993 by Moore [2] in the case of three equal masses and gravitational $-1/r$ potential, using numerical methods. Its existence and stability were later proven formally by way of variational arguments [3], but no closed (analytic) form of this solution has been shown as yet. Moreover, the figure-eight solution has also been found in the general-relativistic three-body dynamics [4], and its bifurcations have been studied as a function of the mass asymmetry [5]. Proofs of existence, as well as some properties of figure-eight orbits in pairwise sums of $-1/r^\alpha$ two-body potentials with $\alpha \neq 1$, have been studied in Refs. [6–8]. Any new solution and/or insight into the existing ones should be of intrinsic interest.

Of course, the figure-eight orbit is highly symmetric, but it is not immediately clear what the reason is for the underlying dynamical symmetry. It is an empirical fact, however, that all known figure-eight orbits exist only in (three-body) permutation-symmetric potentials. Indeed, it is known that the figure-eight orbit bifurcates into new, less symmetric, orbits as one changes the mass ratio(s) of the three particles and thus breaks the permutation symmetry; see Refs. [5], [9]. We explore this connection between the permutation symmetry and the figure-eight orbit and make it more explicit. In the process we have found new solutions with lesser symmetry, much like those in Ref. [9], and obtained new insights into the role of permutation symmetry in the classical three-body problem.

In this paper we report our studies of figure-eight orbits in three kinds of three-body potentials: (i) the Newtonian gravity, i.e., the pairwise sum of $-1/r$ two-body potentials; (ii) the pairwise sum of linearly rising r two-body potentials (also known as the Δ-string potential); and (iii) the Y-junction string potential [10,11] that contains both a genuine three-body part, as well as two-body contributions (this is the first time that the figure-eight has been found in these string potentials, to our knowledge). These three potentials share two common features, viz. they are attractive and symmetric under permutations of any two or three particles.[1]

A set of variables makes this permutation symmetry manifest and we use them to plot the motion of a numerically calculated figure-eight orbit. As there are three independent three-body variables, and there can be at most two independent permutation-symmetric three-body variables,[2] the third variable cannot be permutation symmetric. In other words, the third variable must change under permutations. Moreover, it must be a continuous variable and not be restricted only to a discrete set of points, as is natural for permutations. Thus it must provide a smooth interpolation between (discrete) permutations. We identify here the third independent variable as $\phi = \arctan(\frac{2\rho\cdot\lambda}{\lambda^2-\rho^2})$ and show that it grows/descends (almost) linearly with the time t spent on the figure-eight trajectory and reaches $\pm 2\pi$ after one period T. Thus, ϕ is, for most practical purposes, interchangeable with the time variable t on the

[*]suki@ipb.ac.rs
[†]dmitrasin@ipb.ac.rs

[1]The Coulomb interaction among three identical charged particles is permutation symmetric but repulsive.

[2]There are two irreducible one-dimensional representations of the permutation group s_3.

figure-eight orbit. The hyperangle ϕ is the continuous braiding variable that interpolates smoothly between permutations and thus plays a fundamental role in the braiding symmetry of the figure-eight orbits [2,12].

We then construct the hyperangular momentum $G_3 = \frac{1}{2}(\mathbf{p}_\rho \cdot \boldsymbol{\lambda} - \mathbf{p}_\lambda \cdot \boldsymbol{\rho})$ conjugate to ϕ, the two forming an (approximate) pair of action-angle variables for this periodic motion. Here we calculate numerically and plot the temporal variation of ϕ, as well as that of the hyperangular momentum $G_3(t)$, the hyper-radius $R(t)$ and $r(t)$. We show that the hyper-radius $R(t)$ oscillates about its average value $\overline{R}$ with the same angular frequency ($3\dot{\phi}$) and phase, as the new ("reduced area") variable $r(t)$. Thus, we show that $\phi(t)$ is, for most practical purposes, interchangeable with the time variable t, in agreement with the tacit assumption(s) made in Refs. [3,7], though the degree of linearity of this relationship depends on the precise functional form of the three-body potential; see Sec. III B.

As stated above, ϕ is not exactly proportional to time t but contains some nonlinearities that depend on the specifics of the three-body potential; consequently, the hyperangular momentum G_3 is not an exact constant of this motion but oscillates about the average value $\overline{G}_3$, with the same basic frequency $3\dot{\phi}$. Thus, the time-averaged hyperangular momentum $\overline{G}_3$ is the action variable conjugate to the linearized hyperangle ϕ'.

We use these insights to characterize two new planar periodic, but not choreographic, three-body motions with vanishing total angular momentum. One of these orbits corresponds to a modification of the figure-eight orbit with $\phi(t)$ that also grows more or less linearly in time but has a more complicated periodicity pattern defined by the zeros of the area of the triangle formed by the three particles (also known as "eclipses," "conjunctions," or "syzygies"). Another new orbit has $\phi(t)$ that grows in time up to a point and then stops and "swings back." We show that this motion, and the other two, can be understood in view of the analogy between the three-body hyperangular ("shape space") Hamiltonian on one hand and a variable-length pendulum in an azimuthally periodic in-homogeneous gravitational field, on the other.

This paper is divided into five parts: after the Introduction in Sec. II we introduce a complete (maximal) set of permutation-symmetric three-body variables and illustrate them with two examples: (i) the curves in the "shape space" of triangles depicting those triangles with one of its three angles equal to a particular value in the range $(\frac{\pi}{3},\pi)$ and (ii) the contour plots of the Newtonian gravity, the Y-junction string, and the Δ-string potentials. In Sec. III we show the time dependence of the figure-eight motion in Newton's gravity and the Y-string potentials. In Sec. IV we show and discuss the new solutions. Finally, in Sec. V, we summarize and draw conclusions.

II. PERMUTATION-SYMMETRIC THREE-BODY COORDINATES

As the static three-body potential depends on three independent scalar variables, e.g., the pairwise relative distances/separations, the choice of appropriate (relative) variables is a crucial one. A number of three-body relative variables have been devised, starting with those introduced by C. G. Jacobi in the 19th century [13] and extending to the so-called hyper-spherical coordinates introduced in the 1960s [14–16]. These variables were introduced in attempts at solving certain quantum mechanical three-body problems that demand special attention to be paid to the permutation symmetry. Nevertheless, only one, Ref. [14], of these sets is manifestly permutation symmetric and yet it has not been widely used.

Here we use the manifestly permutation-symmetric three-body variables, apparently first introduced by Hopf: the hyper-radius R, the "scale-invariant area" of the triangle $\sqrt{1-r^2} = 2R^{-2}|\boldsymbol{\rho} \times \boldsymbol{\lambda}|$, where we find as the hyperangle $\phi = \arctan(\frac{2\rho\cdot\lambda}{\lambda^2-\rho^2})$, which is conjugate to the generalized hyperangular momentum $G_3 = \frac{1}{2}(\mathbf{p}_\rho \cdot \boldsymbol{\lambda} - \mathbf{p}_\lambda \cdot \boldsymbol{\rho})$. One may relate these to the hyperspherical variables $x' = \frac{2\rho\cdot\lambda}{R^2}$ and $z' = \frac{\lambda^2-\rho^2}{R^2}$ that have the circle with unit radius as their natural domain. Then the area of the triangle $\frac{\sqrt{3}}{2}|\boldsymbol{\rho} \times \boldsymbol{\lambda}|$ and the hyper-radius R are related to the the new variables r, ϕ as follows:

$$r^2 = (x'^2 + z'^2) = 1 - \left(\frac{2|\boldsymbol{\rho} \times \boldsymbol{\lambda}|}{R^2}\right)^2 \tag{1}$$

$$\phi = \tan^{-1}\left(\frac{x'}{z'}\right). \tag{2}$$

The hyperangle ϕ is zero at the $(x = 0, z = 1)$ point ("12 o'clock") and increases as one moves clockwise.

A. The shape space of triangles

The natural domain of the permutation-symmetric variables is a circle with unit radius; see Fig. 1. The points on the unit circle correspond to collinear configurations ("triangles" with zero area).

The two straight lines at angles of $\pm\frac{2\pi}{3}$, together with the vertical axis, are the three (reflection) symmetry axes; these reflections correspond to the three "two-body permutations"/transpositions in the s_3 permutation group. The two cyclic permutations of the s_3 permutation group correspond to the rotations through $\pm\frac{2\pi}{3}$.

The six points where the symmetry axes cross the big circle in Fig. 1 correspond to either (a) three collinear configurations ("shapes") in which one pair of particles has vanishing separation (big solid circles), i.e., "sits on top of each other," or (b) three collinear configurations ("shapes") in which one particle has equal separation from the other two, i.e., "sits in the middle between the other two" (small solid circles). The center of the circle corresponds to the equilateral triangle configuration ("shape"), which turns into a point when the hyper-radius $R \to 0$

B. Newton's, Δ, and Y-string potentials

In Figs. 2, 3, and 4 we show three attractive three-body potentials that are either pairwise sums of two-body terms, viz. Newton's

$$V_{\text{Newton}} = -g\sum_{i<j}^{3}\frac{1}{|\mathbf{x}_i - \mathbf{x}_j|}, \tag{3}$$

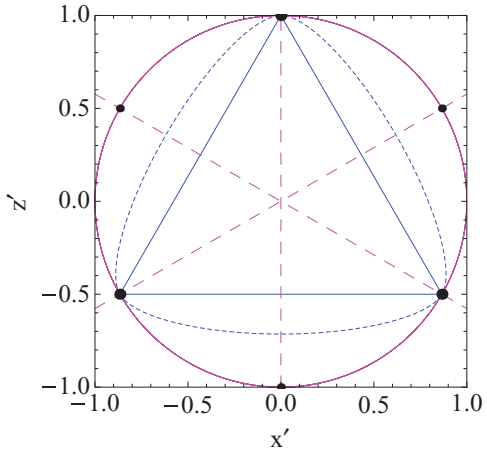

FIG. 1. (Color online) The curves and lines in shape space of triangles depicting triangles with one fixed angle: (a) the outer blue (short dashed) line, for the fixed angle equal to 109.5°; (b) blue (solid) lines for the fixed angle equal to $\frac{\pi}{2}$, as functions of $z' = z = \cos 2\chi$ (ordinate = vertical axis) and $x' = x\sqrt{1-z^2} = \cos\theta \sin 2\chi$ (abscissa = horizontal axis). The domain of these variables is a magenta (dark gray) circle of radius unity. The two straight red (long dashed) lines at angles of $\pm\frac{2\pi}{3}$, and the vertical axis are the symmetry axes, i.e., s_2 subgroups of the s_3 permutation group, and of the "constant angle curves" in shape space, as well. The three collinear configurations in which one pair of particles has vanishing separation are denoted by big solid circles, and the three collinear configurations in which one particle has equal separations from the other two are denoted by small solid circles.

and the Δ string

$$V_\Delta = \sigma_\Delta \sum_{i<j}^{3} |\mathbf{x}_i - \mathbf{x}_j|, \tag{4}$$

or contain such a two-body component in a limited part of the configuration (shape) space, such as the Y string

$$V_Y = \sigma_Y \min_{\mathbf{x}} \sum_{i=1}^{3} |\mathbf{x_i} - \mathbf{x}| = \sigma_Y \sum_{i=1}^{3} |\mathbf{x_i} - \mathbf{x_T}|, \tag{5}$$

where the minimum of the sum occurs at the Torricelli point $\mathbf{x} = \mathbf{x_T}$; see Ref. [11].

Note that the Y-string potential has perfectly concentric contour lines within a pear-shaped region of shape space delineated by the blue dashed line in Fig. 2. As shown in Ref. [17], that "hyper-rotational" symmetry leads to a new constant of motion in this part of shape space. A clear discrimination of the Y-string from the Δ-string three-quark potentials had been a problem in lattice QCD until Ref. [17] showed that the two kinds of potentials have essentially different hyperangular dependencies. The separation of one kind of three-body potential from another is facilitated by the use of the new variables r and ϕ. Then the Y-string component is manifested through the sole dependence on r, whereas the Δ string is manifested through the dependence of the potential on the hyperangle ϕ, within the confines of the "central potential" boundary in terms of "old" variables (χ,θ) [10].

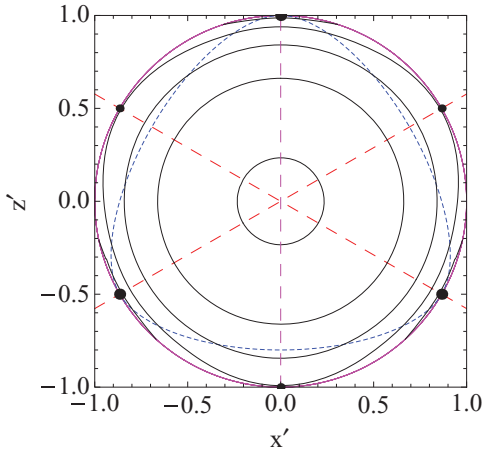

FIG. 2. (Color online) The equipotential contours for the central Y-string potential, and the boundary between the central Y-string and two-string potentials as functions of $z' = z = \cos 2\chi$ (vertical axis) and $x' = x\sqrt{1-z^2} = \cos\theta \sin 2\chi$ (horizontal axis). The blue (short dashed) curve denotes the boundary between the two-body and the three-body components of this potential; see Ref. [10]. The rotation symmetry about the axis pointing out of the plane of the figure should be visible to the naked eye.

Note that all three potentials in Figs. 2, 3, and 4 have essentially (topologically) the same form in the two hyperangular ("shape space") variables:

$$V(r,\phi) = V(r) + \delta V(r)\cos(3\phi) + \cdots. \tag{6}$$

This is a consequence of their permutation symmetry. Any attractive permutation-symmetric potential has its highest value at the center of the circle ($r = 0$) and it decreases monotonically as one moves radially toward the $r = 1$ circle. Moreover, a permutation-symmetric potential is circularly symmetric at the center $[\delta V(0) = 0]$ and is increasingly broken by a periodic ϕ angular ("two-body") component $\delta V(r)\cos(3\phi)$ as one moves radially toward the $r = 1$ circle.

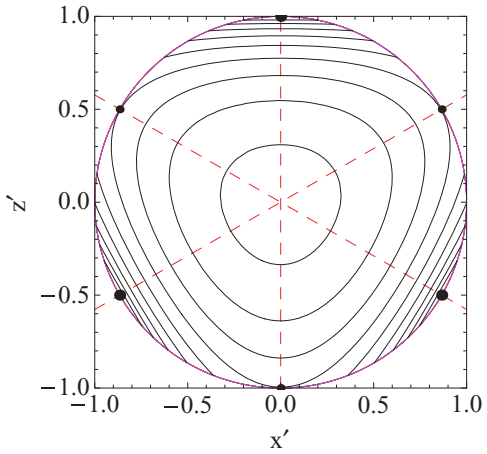

FIG. 3. (Color online) Contour plot of the Δ-string potential as a function of $z' = z = \cos 2\chi$ (vertical axis) and $x' = x\sqrt{1-z^2} = \cos\theta \sin 2\chi$ (horizontal axis) for any fixed value of the hyper-radius R. The rest of the legend is as for Figs. 1 and 2. The center of the circle is the point with the highest value of the potential.

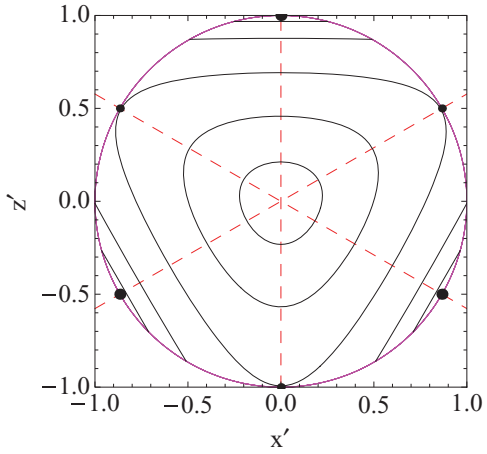

FIG. 4. (Color online) Contour plot of the logarithm of the sum of Newton's two-body potentials as a function of $z' = z = \cos 2\chi$ (vertical axis) and $x' = x\sqrt{1-z^2} = \cos\theta \sin 2\chi$ (horizontal axis) at any fixed value of the hyper-radius R. The rest of the legenda is as in Figs. 1 and 2. As one approaches the two-body collision points (three large solid points on the big circle), the equipotential contour lines become more and more dense and parallel, finally reaching infinite density at these points, due to the singularities (poles) present.

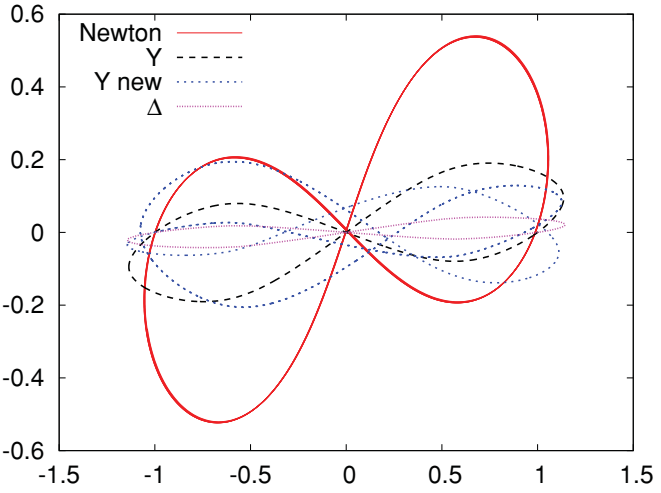

FIG. 5. (Color online) Real-space trajectories of the figure-eight and one new solution that passes through the figure-eight initial configuration for three different potentials. [Red (dark gray) solid curve] Newtonian potential figure-eight; (dark gray long dashed curve) Y-string potential figure-eight; [blue (gray) medium-length dashed curve] Y-string potential new solution; and [magenta (light gray) short dashed curve] Δ-string potential figure-eight.

As a consequence of this "topological equivalence" these potentials lead to certain kinds of orbits, such as the "figure-eight" one, that are essentially identical. The hyper-radial part of the potential does not seem to be very important, so long as it is attractive, because the stability of the orbit is ensured by the approximate (dynamical) O(2) symmetry of these potentials. The details of these potential differ, of course, and therefore lead to different detailed properties of the amplitude and phase variations but not so for the qualitative properties of the motion. Indeed, if the potential does not contain the periodic ϕ-dependent "two-body" component near the "outer edge" of the shape space circle (or near the equator of the shape space hemisphere), then there is no "figure-eight" orbit in that potential.

C. Approximate dynamical O(2) symmetry

The sum of Newton's or Δ-string two-body potentials is approximately symmetric under infinitesimal rotations in the shape space, at least in the central ($r \simeq 0$) part of the "shape space," as can be seen in Figs. 3 and 4, whereas the Y string is exactly symmetric in the same region; see Fig. 2. Of course, the two-body potentials are exactly invariant under the finite ("kinematic") rotations through $\phi = \pm\frac{2\pi}{3}$, which correspond to cyclic permutations, as well as under reflections about the three symmetry axes, which correspond to binary/two-body permutations ("transpositions").

Independence of the potential on the variable ϕ is equivalent to its invariance under (infinitesimal) "kinematic rotation" O(2) transformations

$$\delta x' = 2\varepsilon z' \tag{7}$$

$$\delta z' = -2\varepsilon x', \tag{8}$$

or, in terms of the original Jacobi variables,

$$\delta\boldsymbol{\rho} = \varepsilon\boldsymbol{\lambda} \tag{9}$$

$$\delta\boldsymbol{\lambda} = -\varepsilon\boldsymbol{\rho}. \tag{10}$$

in the six-dimensional hyperspace. This invariance leads to the new integral of motion $G_3 = \frac{1}{2}(\mathbf{p}_\rho \cdot \boldsymbol{\lambda} - \mathbf{p}_\lambda \cdot \boldsymbol{\rho})$, associated with the dynamical symmetry (Lie) group O(2) that is a subgroup of the (full hyperspherical) O(6) Lie group.

This O(2) symmetry transformation is an infinitesimal version of the "kinematic rotations," see Ref. [14], that operate in two ordinarily different planes at the same time[3]: (a) in the plane of Jacobi vectors $\boldsymbol{\rho},\boldsymbol{\lambda}$ and (ii) in the plane of Jacobi momenta $\mathbf{p}_\rho - \mathbf{p}_\lambda$ (these two planes need not coincide in general). It is only in the special case of planar motions that these two planes coincide, and it is only in the (even more special) case of vanishing (total) angular momentum that the new constant of motion has presently discernible consequences.

In the case of the sum of two-body potentials, such as the Newtonian gravity or the Δ-string potential, this generalized hyperangular momentum G_3 is not an exact integral of motion but an approximate one. The precise consequences of such an approximate symmetry depend on the initial conditions of motion, as we shall see below.

III. FIGURE-EIGHT MOTION

A periodic "figure-eight" orbit (Fig. 5), with vanishing total angular momentum ($L = 0$) has been found by Moore [2] in the case of equal masses and gravitational potential.It was shown in Ref. [6] that the hyper-radius R is close to being constant along the figure-eight trajectory: It makes only small-amplitude oscillations in lockstep, i.e., with the same

[3]An ordinary space rotation rotates both position and velocity vectors about the same axis and through the same angle.

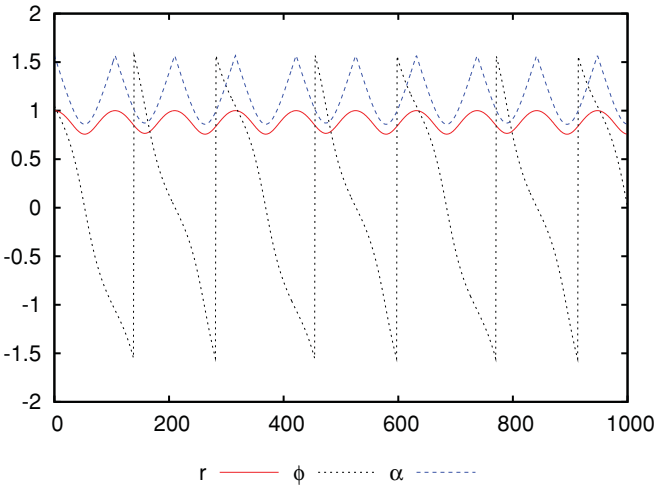

FIG. 6. (Color online) The time dependence of the hyperangular radius r red (solid) and the hyperangles $\alpha = \sin^{-1} r$ [blue (long-dashed) line] and ϕ [gray (short-dashed) line] of the figure-eight solution in Newton's potential.

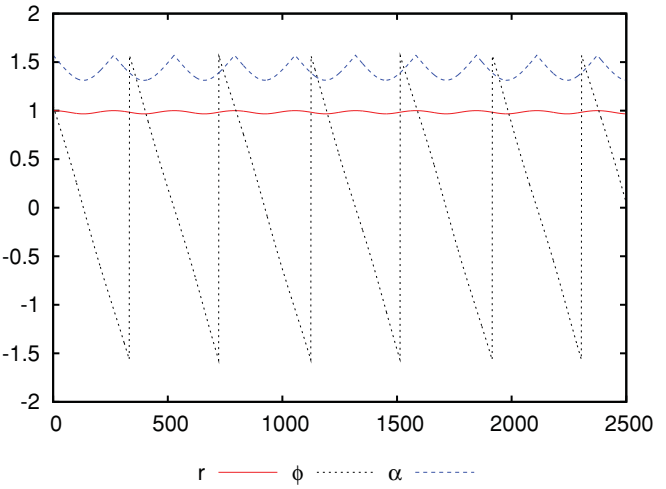

FIG. 7. (Color online) The time dependence of the hyperangular radius r red (solid) and the hyperangles $\alpha = \sin^{-1} r$ [blue (long-dashed) line] and ϕ [gray (short-dashed) line] of the figure-eight solution in the Y-string potential.

frequency and locked in phase, with the area of the triangle and the hyperangle ϕ; see below.

A. Time dependence of the hyperangular motion

We take $(r_{\text{init.}}, \phi_{\text{init.}}) = (1, \frac{1}{3}\pi)$ as the initial condition, which is one of three identical configurations, up to permutations. This is a collinear configuration with one particle in the middle of the other two. The initial velocities are such that the total angular momentum vanishes, see Table I.

1. Newtonian gravity

In Fig. 6 we see that both hyperangular variables (r,ϕ) oscillate with the same frequency and locked in phase along the figure-eight trajectory.

2. The Y- and Δ-string potentials

A similar situation is present in the other two potentials: the hyper-radius $R(t)$ is almost constant along this trajectory: it makes small-amplitude oscillations in phase with the area of the triangle, Fig. 7 (similarly for the Δ string, see Fig. 8).

B. Hyperangular ϕ dependence

One can see in Fig. 9 that the periodicity of the figure-eight motion is determined by the braiding angle ϕ.Here one can also see that the actual path in the shape space, Fig. 9, taken by the Newtonian three-body system is remarkably close to the Newtonian isopotential lines in Fig. 4. If this were exactly true, then the hyper-radius would be constant along the figure-eight orbit, but it is not: $R(t)$ and $r(t)$ are periodic functions, with the same basic frequency of $3\phi(t)$ and locked in phase, i.e. they oscillate about their average values as follows

$$\begin{aligned} \phi &= \langle\dot{\phi}\rangle t + \delta\phi \sin(3\phi) + \cdots \\ r(\phi) &= \bar{r} + \delta r \sin(3\phi) + \cdots \\ R(\phi) &= \overline{R} + \delta R \sin(3\phi) + \cdots . \end{aligned} \tag{11}$$

This phase- and frequency locking provide an important constraint that effectively reduces the number of independent degrees of freedom to two. In other words ϕ is the (approximate) cyclic, or "ignorable" variable of the figure-eight periodic motion that may be integrated out/ignored/. The conjugate action variable G_3 is the associated (approximate) integral of motion.

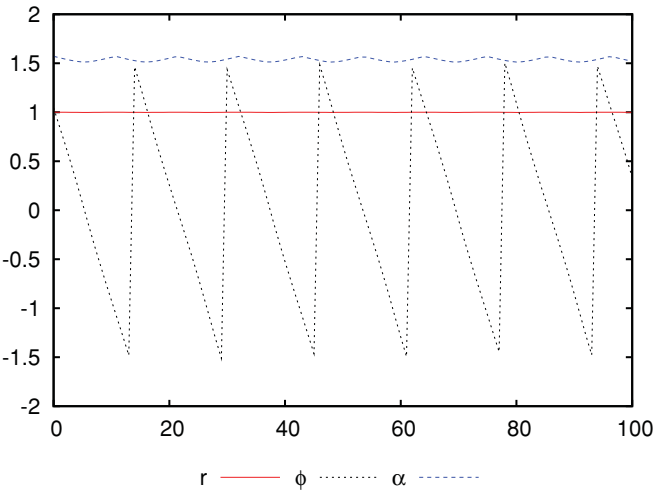

FIG. 8. (Color online) The time dependence of the hyperangular radius r red (solid) and the hyperangles $\alpha = \sin^{-1} r$ [blue (long-dashed) line] and ϕ [gray (short-dashed) line] of the figure-eight solution in the Δ-string potential.

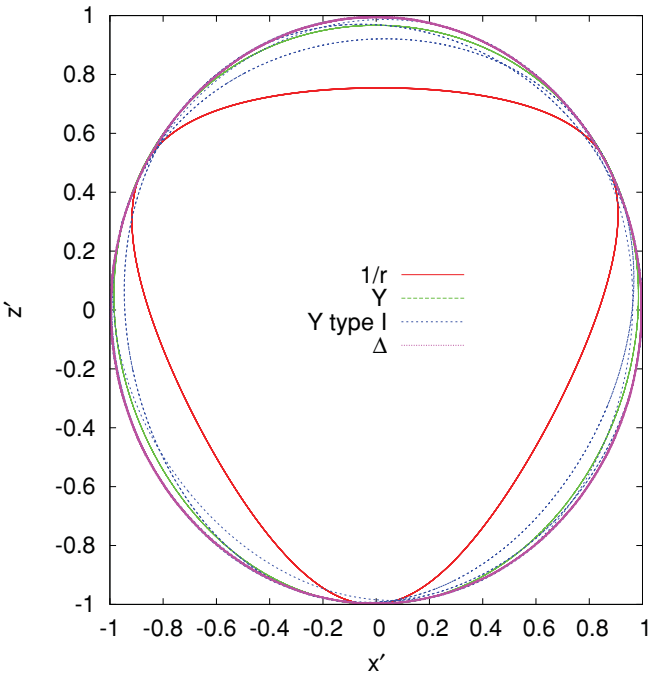

FIG. 9. (Color online) Trajectories of the figure-eight and one new solution in three different potentials in terms of $z' = z = \cos 2\chi$ (vertical axis) and $x' = x\sqrt{1-z^2} = \cos\theta \sin 2\chi$ (horizontal axis). [Red (dark gray) solid curve] Newtonian potential figure-eight; (dark gray long-dashed curve) Y-string potential figure-eight; [blue (gray) medium-length dashed curve] Y-string potential new solution; [magenta (light gray) short-dashed curve] Δ-string potential figure-eight; [magenta (dark gray) solid curve] unit circle.

C. The action variable conjugate to ϕ

In order to find the appropriate action variable we look at the ("kinematic") hyper-angular momentum G_3 that reads

$$G_3 = \frac{m}{4}(Rr)^2\dot{\phi} = \frac{m}{4}(R\sin\alpha)^2\dot{\phi} \tag{12}$$

(with vanishing angular momentum $L = 0$) as a function of permutation-symmetric variables R,$r = \sin\alpha$ and ϕ and oscillates as a periodic function of the hyperangle 3ϕ. Hence, it follows that G_3 and $\dot{\phi}$ must be (almost) constant in orbits with $L = 0$, $R \simeq$ const., and $r \simeq 1$. In other words, the angle ϕ grows (or decreases, depending on the orientation of the motion) almost linearly in time, which is confirmed by our numerical results.

The time/hyperangle average $\overline{G}_3$

$$\overline{G}_3 = \frac{1}{T}\int_0^T G_3 dt = \frac{1}{T}\int_0^T \frac{m}{4}(Rr)^2\dot{\phi}dt = \frac{1}{2\pi}\int_0^{2\pi}\frac{m}{4}(Rr)^2 d\phi \tag{13}$$

is a nonvanishing constant on the figure-eight orbit, furnishing the (approximate) action variable that goes together with the (linearized) hyperangle ϕ for this periodic motion. The approximate constancy of $G_3 \simeq \overline{G}_3 \neq 0$ is the cause of dynamical stability of the figure-eight orbit: The vanishing angular momentum ($L = 0$) three-body relative motion kinetic energy

$$T_{\rm kin} = \frac{m}{2}\left\{\dot{R}^2 + \left(\frac{R}{2}\right)^2\left[\frac{\dot{r}^2}{1-r^2} + (r\,\dot{\phi})^2\right]\right\} = \frac{m}{2}\left\{\dot{R}^2 + \left(\frac{R}{2}\right)^2[\dot{\alpha}^2 + (\dot{\phi}\,\sin\alpha)^2]\right\} \tag{14}$$

has the form of the single-particle kinetic energy in polar coordinates, albeit with polar radius $\frac{R}{2}$ reduced by half in the "hyperangular kinetic energy" $\frac{m}{2}(\frac{R}{2})^2[\dot{\alpha}^2 + (\dot{\phi}\,\sin\alpha)^2]$. This means that another (hyper-) angular-momentum-like three vector **G** is conserved when the potential does not depend on the two angles (α, ϕ).

In the case when the potential depends on α but does not depend on ϕ, or has only small variations with ϕ, then the "azimuthal hyperangular momentum" $G_3 = \frac{\partial T_{\rm kin}}{\partial\dot{\phi}}$ is approximately constant:

$$\dot{G}_3 = -\frac{\partial V(r,\phi)}{\partial\phi} = 3\delta V(r)\sin(3\phi) + \cdots.$$

Then $G_3 \simeq \overline{G}_3 \neq 0$ provides a repulsive term $\frac{2G_3^2}{mR^2}$ in the effective hyper-radial potential $V_{\rm eff}(R) = \frac{2G_3^2}{mR^2} + V_{3-\rm body}(R)$ that prevents the system from collapsing to a point, just as the (ordinary) angular momentum $L \neq 0$ does in the two-body problem.

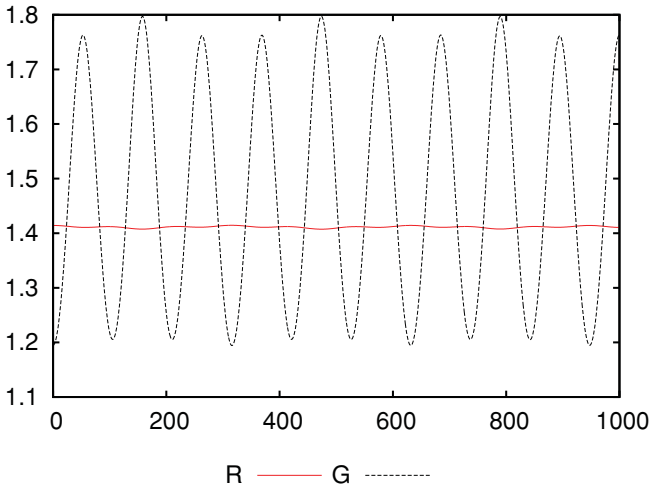

FIG. 10. (Color online) The time dependence of the hyper-radius R (red solid line) and the hyper-angular momentum G (gray dashed line) of the figure-eight solution in Newton's potential. The legenda are explicitly shown below the figure.

1. *Newtonian gravity*

The temporal variation of the hyper-radius $R(t)$ and the hyperangular momentum $G(t)$ in the Newtonian gravitational potential are shown in Fig. 10.

2. *The Y- and Δ-string potentials*

The temporal variation of the hyperangular momentum $G(t)$ and $R(t)$, the former reduced by factor 3 to emphasize

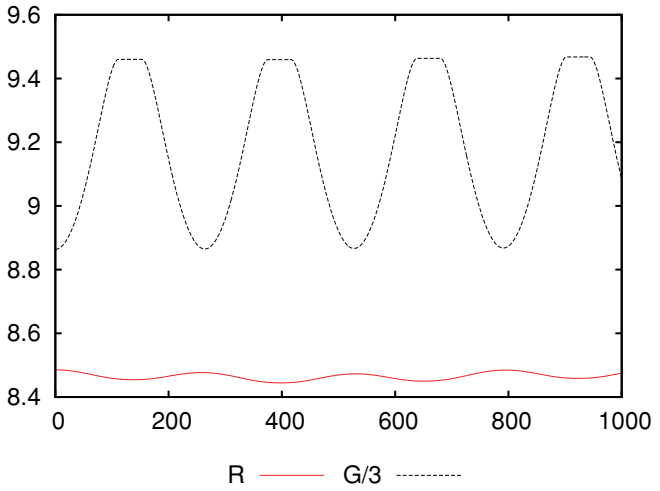

FIG. 11. (Color online) The time dependence of the hyper-radius R (red solid line) and one-third of the hyperangular momentum $G/3$ (gray dashed line) of the figure-eight solution in the Y-string potential.

the small variation of R in the Y-string potential, are shown in Fig. 11.

Note the cutoff peaks of the sines ("flat tops") of the hyperangular momentum $G/3$ due to the exact dynamical O(2) symmetry in that part of the configuration space.

IV. NEW Y-STRING PERIODIC ORBITS

Note, moreover, that the permutation-symmetric three-body potential $V_{3-\text{body}}(\sin\alpha,\phi)$ in the region of the figure-eight orbit [i.e., on the outer fringes of the $(r=\sin\alpha,\phi)$ circle] is attractive as a function of $r=\sin\alpha$, with a minimum at the unit circle ($r=1$) and a strictly periodic function of the (triple) hyperangle 3ϕ.

It should be no surprise, then, that the figure-eight motion of the three-body system, with its almost constant hyper-radius R, has many similarities with that of the spherical pendulum in an inhomogeneous (azimuthally periodic) gravitational field: figure-eight orbit corresponds to rotations, but there are other qualitatively different kinds of motions that we shall display and briefly discuss in this section.

There is a small, yet pronounced, nonlinearity in the figure-eight motion's ϕ's temporal dependence, particularly near the $\phi=0,\pm\frac{2\pi}{3}$ points. These three points/lines in the (r,ϕ) circle (see Fig. 9) correspond to the configurations of closest two-body approach in real space. Of course, the figure-eight orbit does not touch the "unit circle" at these three values of ϕ, so there are no two-body collisions in this type of orbit.

Yet, this suggests that there might be other, perhaps multiply periodic, solutions with "trajectories" in the (r,ϕ) plane that touch the $r=1$ circle at the hyperangle values other than $\phi=\pm\frac{\pi}{3},\pi$ and/or approach the unit circle (the equator of the shape hemisphere) even closer to the two-body collision points. The latter fact means that the corresponding trajectories in real space are "narrower" than the figure-eight one.

We have studied this region more closely and found several new periodic solutions with lesser symmetry than the figure-eight one that pass through the "infinitesimal" neighborhood of the initial state but only in the Y-string and the Δ-string potentials (i.e., not in Newton's gravity, as yet). We display two interesting new orbits below. The initial conditions are given in Table I.

TABLE I. The initial conditions for the solutions shown in this paper: d is the value of the initial distance between the outer left (or right) particle and the middle one and the velocities (both are in dimensionless units where the masses and the coupling constants have been set equal to unity); the angle θ is in radians.

Name	d	v	θ(rad)	Potential
Fig. 8	6	1.37	1.205	Y string
Type I	6	1.32	1.437	Y string
Type II	6	4.53	1.40	Y string
Fig. 8	1	0.6355	0.5736	Newton
Fig. 8	1	0.536	1.49287	Δ string

A. Type I ("linear-in-ϕ") reduced symmetry solution

First, note that the real-space trajectory of ("right-hand-side") particle number 1 in Fig. 12 differs from the one of the ("central") particle number 2 in Fig. 13, thus making it clear that this is a periodic, but not a choreographic, motion.

In other words, this solution is symmetric "merely" under the two-body permutation group s_2 rather than under the three-body permutation group s_3. Due to the reduced symmetry, one particle executes an "independent" motion, whereas the other two move on orbits that are mirror images of each other, very much like those in Ref. [9]. This means that this new solution is probably a bifurcation of the figure-eight orbit as a function of particle masses related to those found in the Ref. [5], i.e., as a function of explicit s_3 permutation symmetry breaking.

The figure-eight orbit touches the unit circle at three points of the equilateral triangle defined by $\phi=\pm\frac{1}{3}\pi,\pi$ (see Fig. 9), whereas this new solution touches it at only one vertex of this equilateral triangle viz. $\phi=\frac{1}{3}\pi$, and "cuts corners" at the other two, only to touch the unit circle at four other values of ϕ that differ from the two-body collisions points $0,\pm\frac{2}{3}\pi$. This is still a periodic solution with a period of 8π, i.e., it takes four cycles

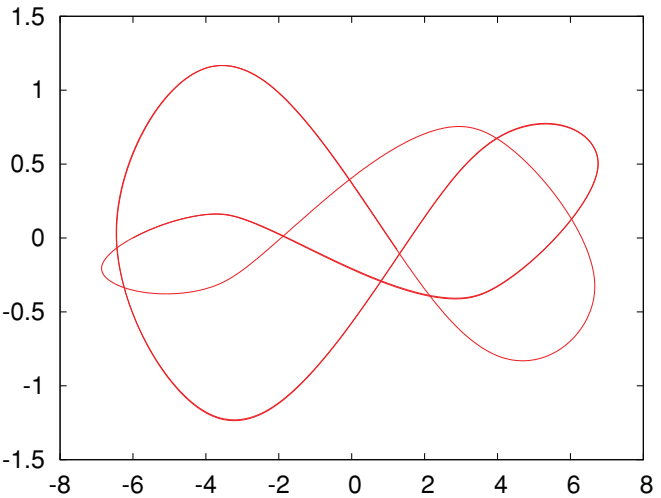

FIG. 12. (Color online) Real-space trajectory of particle number 2 of the type I new solution that passes through the figure-eight initial configuration.

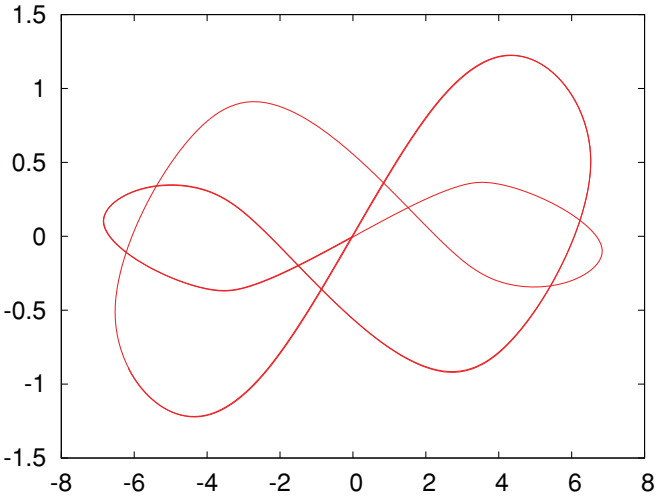

FIG. 13. (Color online) Real-space trajectory of particle number 1 of the type I new solution that passes through the figure-eight initial configuration. The trajectory of particle number 3 is a reflection about the line dividing this trajectory vertically.

of the hyperangle ϕ to complete one period, but with several different hyperangular frequencies, instead of the single basic frequency 3ϕ. This fact may not be immediately visible to the naked eye, as these frequencies are close to 3ϕ, but shows up as "beats" in the time dependence of the amplitudes.

The hyperangle ϕ in this solution (still) grows (or descends) indefinitely, so this solution also corresponds to a kind of rotation of the pendulum, but with a changing angular velocity, see Fig. 14.The time derivatives show the beats more clearly; see Fig. 15.The temporal variation of the hyper-radius $R(t)$ is

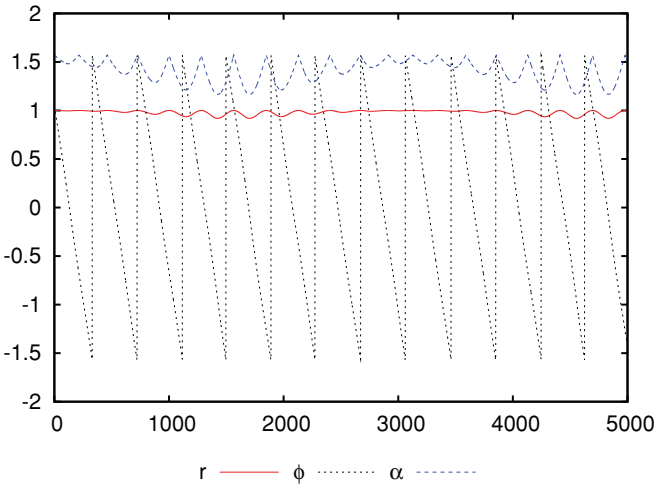

FIG. 14. (Color online) The time dependence of the hyperangular radius r (red solid line), and the hyperangles $\alpha = \sin^{-1} r$ [blue (long-dashed) line] and ϕ [gray (short-dashed) line] of the type I new solution in the Y-string potential that passes through the figure-eight initial configuration. Note that ϕ moving from 0 to 2π corresponds to two segments between vertical lines (discontinuities) due to the numerical evaluation of inverse trigonometric functions. Note that one complete period of the motion corresponds to eight such segments, i.e., to ϕ changing from 0 to 8π, or to four complete revolutions around the (r,ϕ) circle.

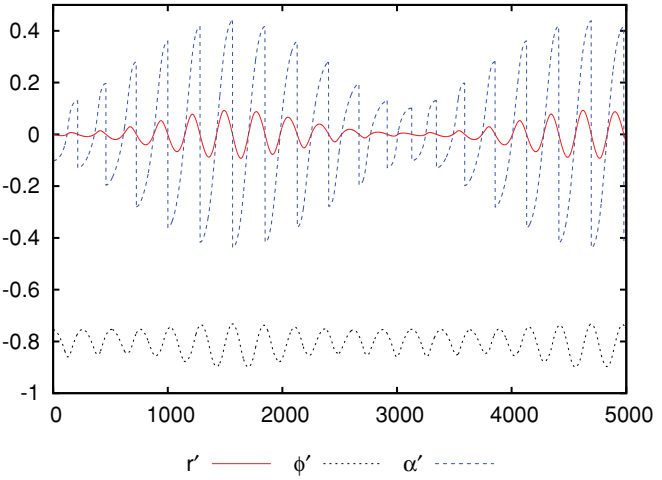

FIG. 15. (Color online) The first derivatives of the time dependence of the hyperangular radius $\dot{r}$ (red solid line), and the hyperangles $\dot{\alpha} = \frac{d}{dt}\sin^{-1} r$ (blue long-dashed line) and $\dot{\phi}$ (gray short-dashed line) of the type-I new solution in the Y-string potential that passes through the figure-eight initial configuration.

shown in Fig. 16 and that of the hyperangular momentum $G(t)$ is shown in Fig. 17.

Note the beats in the time evolution of $R(t)$ and $G(t)$, as discussed.

B. Type II ("oscillating ϕ") reduced symmetry solution

First note that the real-space trajectory of particle number 2 in this solution, Fig. 18, differs from the one of particle number 1, thus making it clear that this is also a periodic, but not a choreographic, motion. The trajectory of particle number 3 (blue online) is a reflection of trajectory of particle number 1 about the origin.

At first, the aforementioned action-angle variables do not seem appropriate for this new periodic orbit; indeed, the (formerly) linear increase (decrease) of the hyperangle ϕ is now subject to substantial modifications: After initial rapid

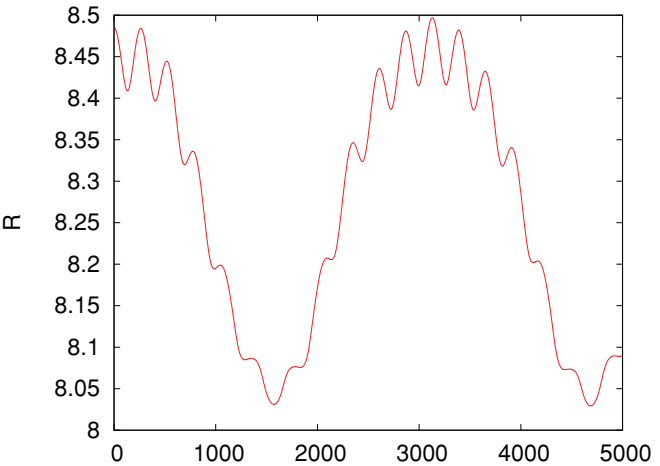

FIG. 16. (Color online) The time dependence of the hyper-radius R of the type I new solution in the Y-string potential that passes through the figure-eight initial configuration.

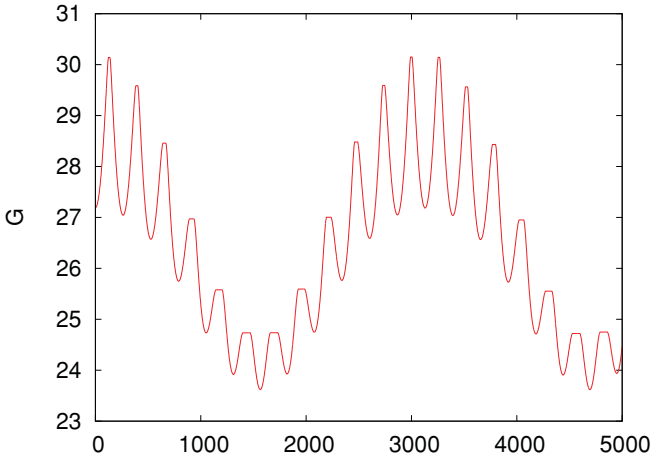

FIG. 17. (Color online) The time dependence of the hyperangular momentum G of the type I new solution in the Y-string potential that passes through the figure-eight initial configuration. Note the cutoff peaks of the sines ("flat tops").

(hyper-) rotation in the clockwise direction starting from $\phi = 0$, it slows down and stops around $\phi_{\min} \simeq -0.764\pi$ (Fig. 19) and then changes the direction of motion and swings back yet again only to stop, this time around $\phi_{\max} \simeq 1.431\pi$, and then repeating this cycle ad infinitum. Note that the maximal difference (twice the amplitude) of ϕ is numerically close to being a simple fraction of π, i.e., $\Delta\phi = \phi_{\max} - \phi_{\min} = 13.0001\frac{1}{6}\pi$, whereas the average value $\overline{\phi} = \frac{1}{2}(\phi_{\max} + \phi_{\min})$ is numerically close to $\frac{1}{3}\pi$. We suspect that $\frac{13}{6}\pi$ and $\frac{1}{3}\pi$ are the exact values and that the deviations from our numerical values are due to rounding-off errors. This resembles the oscillations of a variable-length pendulum. Indeed, Fig. 19 shows that the hyper-radius $R(t)$ is oscillating with the same frequency and phase as the hyperangle $\phi(t)$, thus extending the analogy with the variable-length pendulum model.

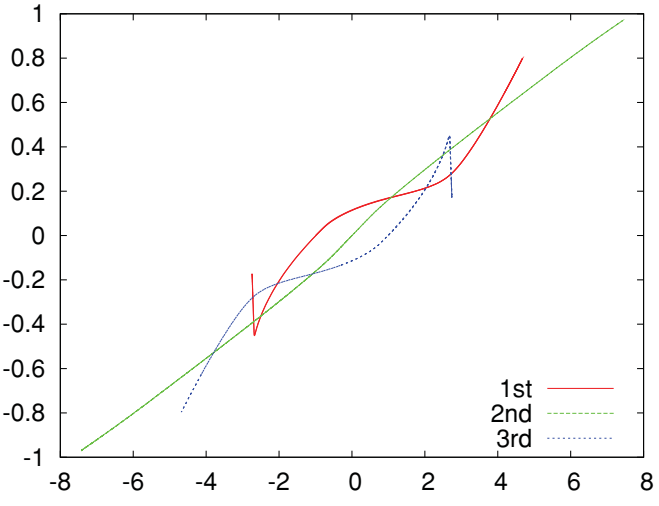

FIG. 18. (Color online) Real-space trajectories of particle number 1 (red solid line), particle number 2 [green (light gray) dashed line], and particle number 3 [blue (dark gray) dashed line] line in the type II new solution that passes through the figure-eight initial configuration.

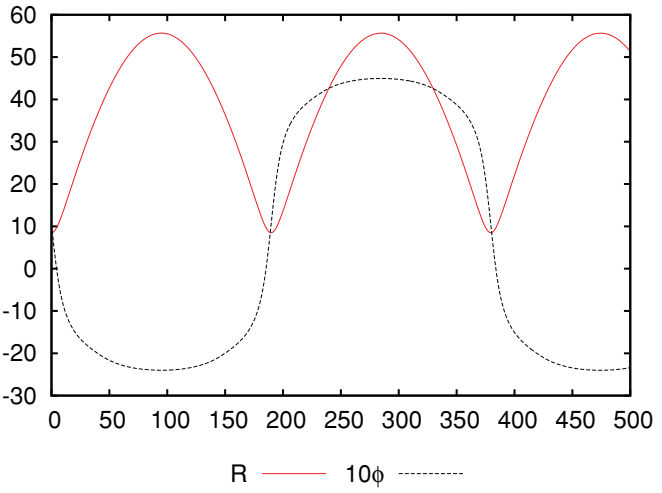

FIG. 19. (Color online) The time dependence of the hyper-radius R (red solid line) and $10\times\phi$ (gray short-dashed line) in the type II "oscillating" solution in the Y-string potential.

V. CONCLUSIONS

We have studied the figure-eight motion in three different three-body potentials in terms of permutation-symmetric variables $(R, r = \sin\alpha)$ and the braiding hyperangle ϕ. The existence of this orbit depends on the periodic dependence of the potential on the braiding hyperangle ϕ that "guides" the figure-eight orbit(s) around the two-body collision points.

The figure-eight orbits in the triangle shape space are generally close to their isopotential lines, although formal arguments show that they cannot be exactly identical [18]. Thus the exact analytic solutions ought to be sought among (small) oscillations about the isopotential lines, with basic frequency 3ϕ. The Hamiltonian of three identical particles in a permutation-symmetric potential with vanishing total angular momentum has certain similarities with that of a spherical pendulum in inhomogeneous azimuthally periodic potentials, which, in turn, suggests existence of other types of solutions.

We have found two new periodic solutions in the Y-string potential that pass through the figure-eight initial state but do not share its symmetry. One of these solutions (type I) has a monotonically rising (descending) hyperangle ϕ, just like the figure-eight orbit, but a different pattern of syzygies, whereas the second (type II) new solution ϕ is oscillating about its average value of $\frac{\pi}{3}$, with the hyper-radius R following suit. All of these orbits are clearly characterized by their (R, r, ϕ) behaviors that display certain similarities, despite their independent and seemingly random form of trajectories in the configuration space. Thus we believe this to be a good set of variables to mathematically simplify and describe all periodic orbits of three identical bodies.

A few words about the history of this subject and our approach to it might be in order now. In our study Ref. [17] of the so-called Y-junction and the Δ-string potentials we found an integral of three-body motion, when the three-body. potential depends on only two, rather than three, independent three-body variables, viz., the hyper-radius (or the moment of inertia divided by the quark/particle mass) and the area of the

triangle defined by the three bodies.[4] As the static three-body potential may depend on (at most) three independent scalar variables, our observation naturally begged the question: What is the third independent three-body variable in this set?[5] It was an attempt to answer this question that brought us to the present permutation-symmetric variables. We are not the first ones to use them, however: Chenciner and Montgomery have used these variables (these authors call θ "our" variable ϕ) to parametrize the triangle shape space in Ref. [3]. According to Ref. [3], H. Hopf was the first one to introduce these variables; Ref. [19].

[4]The exact Y-string potential does not always conserve this new integral of motion, due to its angle-dependent "two-body" parts, but is valid in the major part of the "triangle shape space" and will be shown to play a role in the existence of a new, figure-eight-shaped closed trajectory.

[5]As the first two variables (the hyper-radius and the area of the triangle) are manifestly invariant under permutations of the three particles, we call this set "permutation symmetric."

ACKNOWLEDGMENTS

This work was financed by the Serbian Ministry of Science and Technological Development under Grant No. 141025. One of us (V.D.) wishes to thank A. Ohnishi for hospitality at the Yukawa Institute for Theoretical Physics, Kyoto, where some of this work was carried out. The same author thanks T. Sato and H. Suganuma for valuable conversations.

[1] M. Valtonen, H. Karttunen, *The Three-Body Problem* (Cambridge University Press, Cambridge, 2005).

[2] C. Moore, Phys. Rev. Lett. **70**, 3675 (1993).

[3] A. Chenciner, R. Montgomery, Ann. Math. **152**, 881 (2000).

[4] T. Imai, T. Chiba, and H. Asada, Phys. Rev. Lett. **98**, 201102 (2007).

[5] J. Galán, F. J. Muñoz-Almaraz, E. Freire, E. Doedel, and A. Vanderbauwhede, Phys. Rev. Lett. **88**, 241101 (2002).

[6] T. Fujiwara, H. Fukuda, and H. Ozaki, J. Phys. A **36**, 10537 (2003).

[7] T. Fujiwara, H. Fukuda, and H. Ozaki, J. Phys. A **36**, 2791 (2003).

[8] T. Fujiwara, H. Fukuda, A. Kameyama, H. Ozaki, and M. Yamada, J. Phys. A **37**, 10571 (2004).

[9] R. Broucke, A. Elipe, and A. Riaguas, Chaos, Solitons and Fractals **30**, 513 (2006).

[10] V. Dmitrašinović, T. Sato, and M. Šuvakov, Eur. Phys. J. C **62**, 383 (2009).

[11] T. T. Takahashi, H. Suganuma, Y. Nemoto, and H. Matsufuru, Phys. Rev. D **65**, 114509 (2002).

[12] G. C. Rota, Mathematical Snapshots, Killian Faculty Achievement Award Lecture, 1997.

[13] E. T. Whittaker, *A Treatise on the Analytical Dynamics of Particles and Rigid Bodies* (Cambridge University Press, Cambridge, 1993).

[14] F. T. Smith, J. Chem. Phys. **31**, 1352 (1959); Phys. Rev. **120**, 1058 (1960); J. Math. Phys. **3**, 735 (1962); R. C. Whitten and F. T. Smith, *ibid.* **9**, 1103 (1968).

[15] L. M. Delves, Nucl. Phys. **9**, 391 (1958); **20**, 275 (1960).

[16] Yu. A. Simonov, Sov. J. Nucl. Phys. **3**, 461 (1966) [Yad. Fiz. **3**, 630 (1966)].

[17] V. Dmitrašinović, T. Sato, and M. Šuvakov, Phys. Rev. D **80**, 054501 (2009).

[18] K.-C. Chen, Discrete Cont. Dyn. S. **7**, 85 (2001).

[19] H. Hopf, Math. Ann. **104**, 637 (1931).